J. Iron Steel Res. Int. (2018) 25:268–274
https://doi.org/10.1007/s42243-018-0029-z

ORIGINAL PAPER

# Helium ions irradiation-induced surface damage in Fe-based melt-spun ribbons

Yu-hang Wei[1,2] · Kun Zhang[1,2] · Zi-qiang Zhao[3] · Yan-sen Li[1,2] · Bing-chen Wei[1,2]

Received: 23 August 2017 / Revised: 21 December 2017 / Accepted: 21 December 2017 / Published online: 27 February 2018


**Abstract**
The $Fe_{78}Si_8B_{14}$ and $Fe_{78}P_8B_{14}$ ribbons with different wheel speeds were prepared by melt-spinning, and their responses to $He^+$ ion irradiation were investigated. Previous studies had shown that the ion beam resistance capability of amorphous ribbons was better than their corresponding crystalline counterparts. However, no significant changes on the surface at low fluence are observed. At a relatively higher fluence, both the ribbons prepared at low and high wheel speeds behave the similar irradiation responses: peeling, flaking and multi-layer damages occur. The fully amorphous ribbons prepared at a high wheel speed can accommodate partial incident ions owing to the inherent disordered structure. As the irradiation fluence increases, they fail to accommodate the excess incident ions, which easily aggregate to result in the surface damage. While the partial amorphous ribbons prepared at a low wheel speed possess lots of unstable crystalline grain boundaries owing to the precipitation of Si- or P-rich phase, which may act as the source for the irradiation-induced defects annihilation. Results show that the size and the fraction of precipitate phases in amorphous matrix may play a dominated role in resisting the ion irradiation.

**Keywords** Melt-spinning · Ion irradiation · Fe-based melt-spun ribbon · Damage · Precipitate phase

## 1 Introduction

Bulk metallic glasses (MG) have attracted great interest in recent decades for its unique mechanical and chemical properties such as high strength, large elastic strain and high corrosion resistance [1–6]. Due to their inherent disordered structure, they are supposed to be ideal potential candidates for application in nuclear-irradiated environments or deep space. Besides, the nanocrystalline alloys also exhibit wonderful anti-irradiation performance [7–14]. This attributes to the existence of numerous grain boundaries which act as the "trap" for absorbing the point defects induced by ion beam [12–19]. Thus, there is a great deal of research interest in prefabricating controlled grains in MGs, which may present different irradiation effects owing to the combined role of the MG matrix and nano- or micro-sized precipitated phase. Fe-based melt-spun ribbons fabricated by rapid quenching are found to exhibit superior soft magnetic properties, while different sizes of crystalline phase can be directly formed by controlling the wheel speed. However, there have been few studies on the ion irradiation effects on Fe-based melt-spun ribbons with different wheel speeds. Whether they possess a better anti-radiation performance is worthy to further study.

In this paper, $Fe_{78}Si_8B_{14}$ and $Fe_{78}P_8B_{14}$ melt-spun ribbons with different wheel speeds were prepared by melt-spinning, and their responses to $He^+$ ion irradiation were studied. These aspects of research could help understand the interaction between the matrix and ion beam, which further promote their application in irradiation environment.

## 2 Experimental

The melt-spun ribbons of $Fe_{78}P_8B_{14}$ and $Fe_{78}Si_8B_{14}$ alloys were prepared using a single roller machine (sdj-11) with different wheel speeds (15, 25, 35 and 45 m/s, respectively).

✉ Kun Zhang
zhangkun@imech.ac.cn

✉ Bing-chen Wei
weibc@imech.ac.cn

[1] Key Laboratory of Microgravity (National Microgravity Laboratory), Institute of Mechanics, Chinese Academy of Sciences, Beijing 100190, China

[2] School of Engineering Science, University of Chinese Academy of Sciences, Beijing 101408, China

[3] School of Physics, Peking University, Beijing 100871, China

The raw materials used for alloy had a purity of 99.99%. The alloy was melted through induction heating in a quartz crucible under argon atmosphere, which was completely remelted five times to ensure its chemical composition homogeneity. And then, the molten alloy was ejected by the pressured argon gas from a 0.8-mm-diameter orifice onto a high-speed rotating molybdenum roller cooled by air cooling. The molybdenum roller was polished by 1200 mesh sand paper with a dimension of $\phi$220 mm × 60 mm. After rapid solidification, the phase structures were studied by X-ray diffraction (Rigaku Smart lab Diffractometer) using Co Kα radiation. Prior to irradiation experiments, the surfaces of the samples were mechanically polished to a mirror finish and cleaned ultrasonically. Next, the prepared samples were irradiated at normal incidence with 100 keV $He^+$ ions using the BNU-400 kV electrostatic accelerator. The temperature of the target plate was under 100 °C by wind cooling during the whole irradiation process. The total fluence was about $5 \times 10^{17}$ ions/cm$^2$.

SRIM program (SRIM2008) was carried out to calculate the range of the incident ions and the displacement damage in the target materials. Thermal analyses were performed in differential scanning calorimeter (DSC Netzsch-404C) at a constant heating rate of 20 K/min under argon atmosphere. The morphology of irradiation damage was obtained using a scanning electron microscope (SEM JSM-6460).

## 3 Results and discussion

Figure 1 shows the XRD patterns of $Fe_{78}P_8B_{14}$ and $Fe_{78}Si_8B_{14}$ melt-spun ribbons at different speeds. It is noted that the $Fe_{78}P_8B_{14}$ and $Fe_{78}Si_8B_{14}$ ribbons keep fully amorphous states at the highest wheel speed. With the decrease in the wheel speed, some nano- or micro-sized crystalline phases were precipitated. In $Fe_{78}P_8B_{14}$ melt-spun ribbons, $Fe_2P$ phase is observed. While in $Fe_{78}Si_8B_{14}$ melt-spun ribbons, $Fe_3Si$ phase is obtained. Besides, as the wheel speed decreases, the intensity of the precipitated phase is higher, which means a large number of the precipitated grains are formed.

Figure 2 displays the variation in thickness and width with the wheel speeds for $Fe_{78}P_8B_{14}$ and $Fe_{78}Si_8B_{14}$ melt-spun ribbons. The thicknesses of the $Fe_{78}P_8B_{14}$ and $Fe_{78}Si_8B_{14}$ melt-spun ribbons are decreased from 62 to 33 μm and 67 to 32 μm with the wheel speed increasing from 15 to 45 m/s. Besides, the widths of the $Fe_{78}P_8B_{14}$ and $Fe_{78}Si_8B_{14}$ melt-spun ribbons are decreased from 2.57 to 1.62 mm and 2.42 to 1.64 mm, respectively. The thickness of the ribbon is dependent on the solidification time which is inversely proportional to the wheel velocity [20].

Figure 3 shows the DSC curves of $Fe_{78}P_8B_{14}$ and $Fe_{78}Si_8B_{14}$ melt-spun ribbons prepared at different wheel speeds. Therefore, the amount of the precipitate phase can be calculated by the thermal analyses. It is assumed that the sample prepared at the highest wheel speed (45 m/s) is fully amorphous. The crystallization fractions $x(t)$ of the above-mentioned melt-spun ribbons can be estimated as:

$$x(t) = \frac{\Delta H_f - \Delta H_p}{\Delta H_f} \quad (1)$$

where $\Delta H_f$ is the entropy of fully amorphous sample prepared at the wheel speed of 45 m/s; and $\Delta H_p$ is the entropy of partial amorphous sample prepared at the wheel speeds of 15, 25 and 35 m/s.

Table 1 shows the crystal fraction of $Fe_{78}P_8B_{14}$ and $Fe_{78}Si_8B_{14}$ melt-spun ribbons obtained by Eq. (1). It is found that the crystal fraction increases with the decrease in the wheel speed, which reaches the maximum values 29% for $Fe_{78}P_8B_{14}$ and 11% for $Fe_{78}Si_8B_{14}$ ribbons.

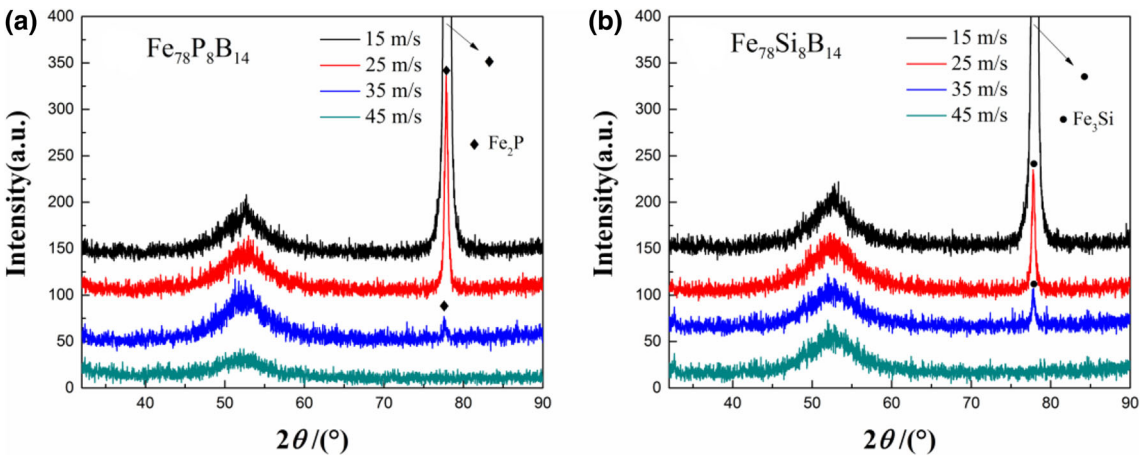


**Fig. 1** XRD patterns of $Fe_{78}P_8B_{14}$ (**a**) and $Fe_{78}Si_8B_{14}$ (**b**) melt-spun ribbons prepared at different speeds

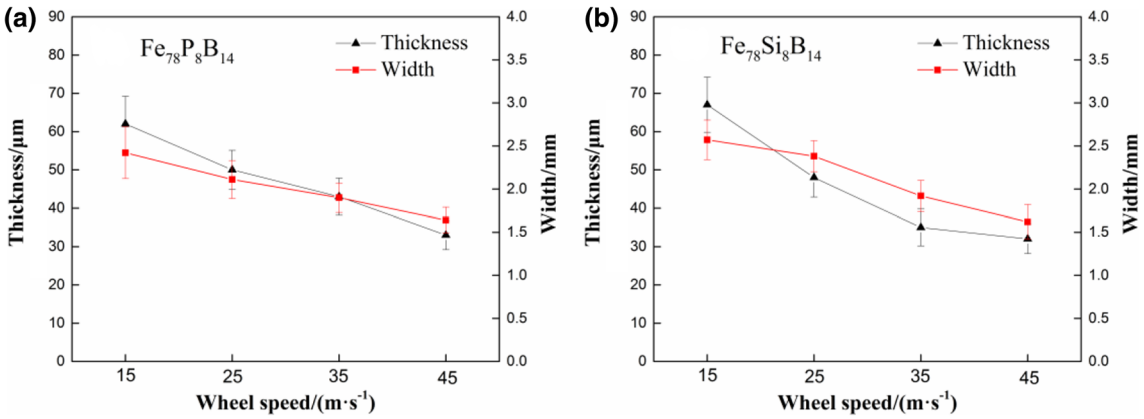


**Fig. 2** Variations in thickness and width with wheel speeds for $Fe_{78}P_8B_{14}$ (**a**) and $Fe_{78}Si_8B_{14}$ (**b**) melt-spun ribbons

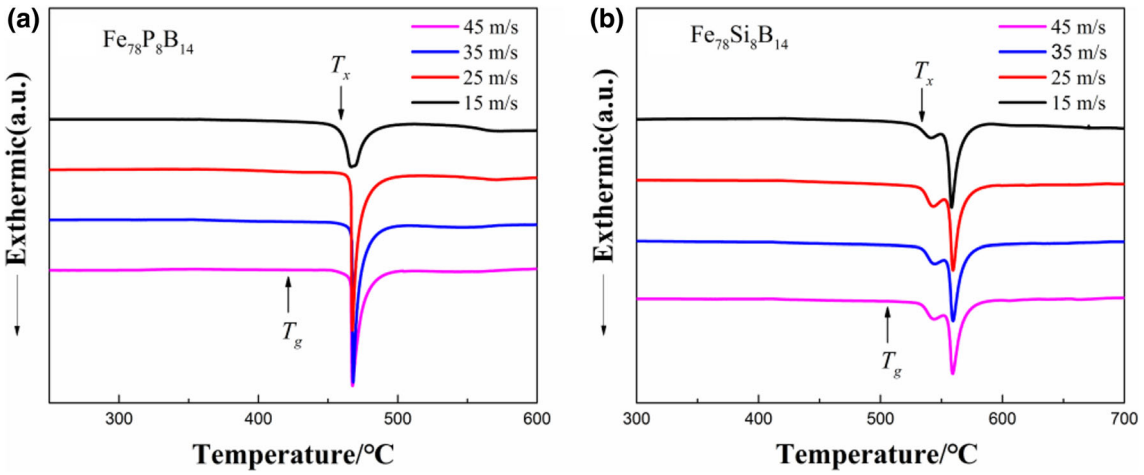


**Fig. 3** DSC curves of $Fe_{78}P_8B_{14}$ (**a**) and $Fe_{78}Si_8B_{14}$ (**b**) melt-spun ribbons prepared at different wheel speeds

**Table 1** Crystal contents of $Fe_{78}P_8B_{14}$ and $Fe_{78}Si_8B_{14}$ melt-spun ribbons

| Wheel speed/(m s$^{-1}$) | 45 | 35 | 25 | 15 |
|---|---|---|---|---|
| Crystal fraction of $Fe_{78}P_8B_{14}$/% | 0 | 4.2 | 19 | 29 |
| Crystal fraction of $Fe_{78}Si_8B_{14}$/% | 0 | 6.5 | 7.5 | 11 |

Figure 4 shows the SEM surface morphology images of $Fe_{78}P_8B_{14}$ and $Fe_{78}Si_8B_{14}$ melt-spun ribbons with a fluence of $2 \times 10^{17}$ ions/cm$^2$. No significant damage on the surface of $Fe_{78}P_8B_{14}$ and $Fe_{78}Si_8B_{14}$ ribbons is observed. In my opinion, ion irradiation can change the structure by increasing the content of free volume in the fully amorphous ribbons (45 m/s). Therefore, the surface of fully amorphous ribbons still keeps smooth. However, the partial amorphous ribbons prepared at lower wheel speeds (15, 25 and 35 m/s) possess lots of unstable crystalline grains owing to the precipitation of $Fe_2P$ and $Fe_3Si$ phases, which may also exhibit an excellent anti-irradiation performance.

Figure 5 shows the SEM photographs of surface morphology of $Fe_{78}P_8B_{14}$ and $Fe_{78}Si_8B_{14}$ melt-spun ribbons at the highest fluence of $5 \times 10^{17}$ ions/cm$^2$. It could be clearly observed that peeling, flaking and multi-layer damages occur on the surface of all melt-spun ribbons after irradiation. As shown in Fig. 5, the un-exfoliated area is black, while the exfoliated area is grey. The un-exfoliated fractions of $Fe_{78}P_8B_{14}$ and $Fe_{78}Si_8B_{14}$ melt-spun ribbons with the different wheel speeds are various. The detailed ratio of the un-exfoliated area to the total irradiated area is calculated in Fig. 6. The largest un-exfoliated ratio is found in wheel speed 35 m/s in both two above-mentioned melt-spun ribbons. As the wheel speed increases to 45 m/s, the irradiation damage becomes more severe again.

In fact, as the irradiation fluence reaches a critical value, the accommodated irradiation-induced defects of the free volume in the fully amorphous ribbons would reach the saturated value. With the continuous increase in the irradiation fluence, the fully amorphous structures fail to

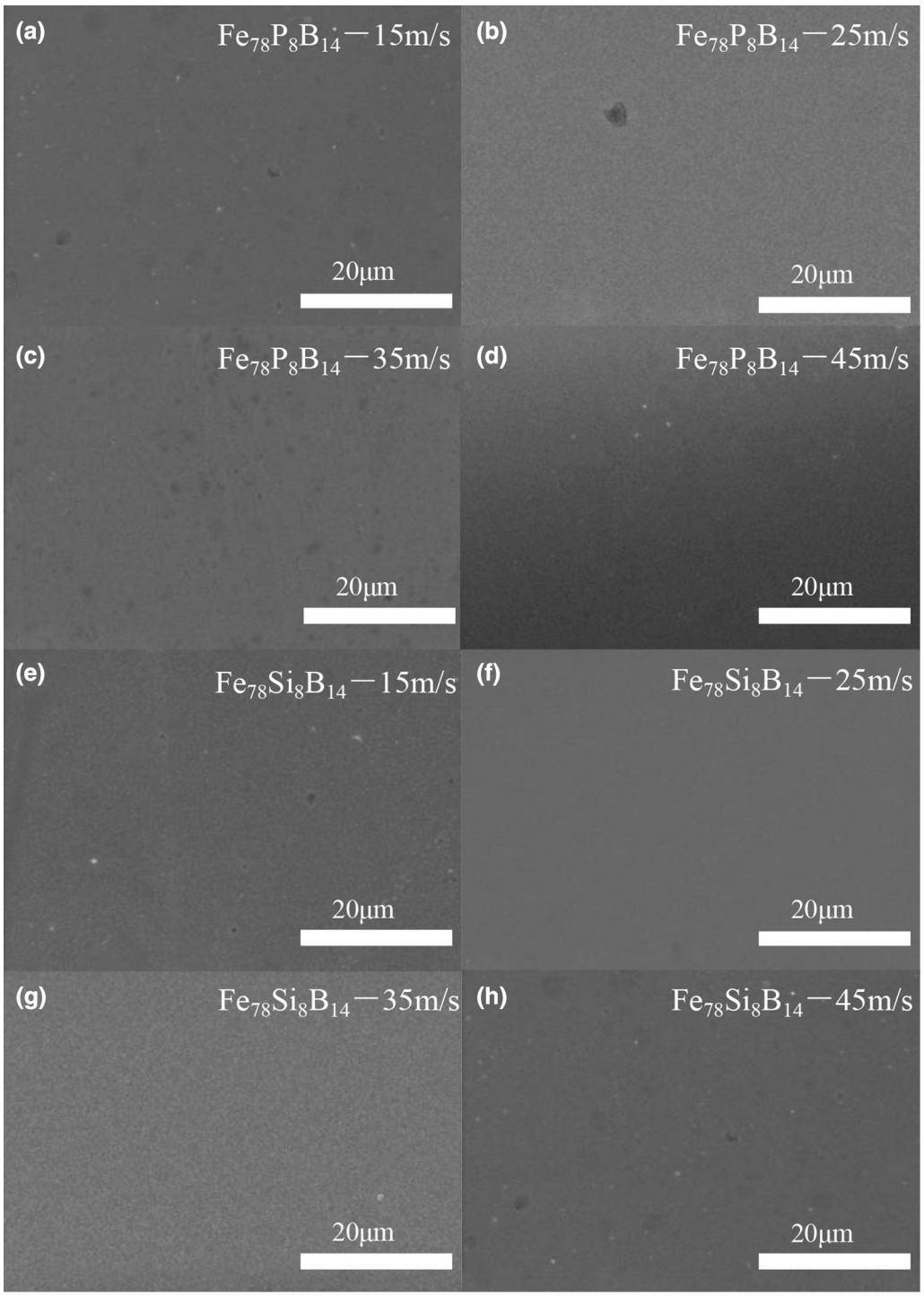


**Fig. 4** SEM images for irradiated $Fe_{78}P_8B_{14}$ (**a–d**) and $Fe_{78}Si_8B_{14}$ (**e–h**) melt-spun ribbons at fluence of $2 \times 10^{17}$ ions/cm$^2$

accommodate the excess irradiation-induced defects and incident ions. Thus, surface damages such as peeling, flaking and multi-layer damage would appear. As shown in Figs. 1 and 3, the structures of the melt-spun ribbons at the wheel speed 35 m/s may possess the relative high density of the grain boundaries in the ribbons owing to the appearance of the sub-micro-sized crystalline phases. Previous studies showed that the grain boundary may act as a source, emitting defects into the amorphous matrix [16–19]. Therefore, the partial amorphous ribbons at the wheel speed of 35 m/s exhibit better anti-radiation performance when compared with the fully amorphous ones.

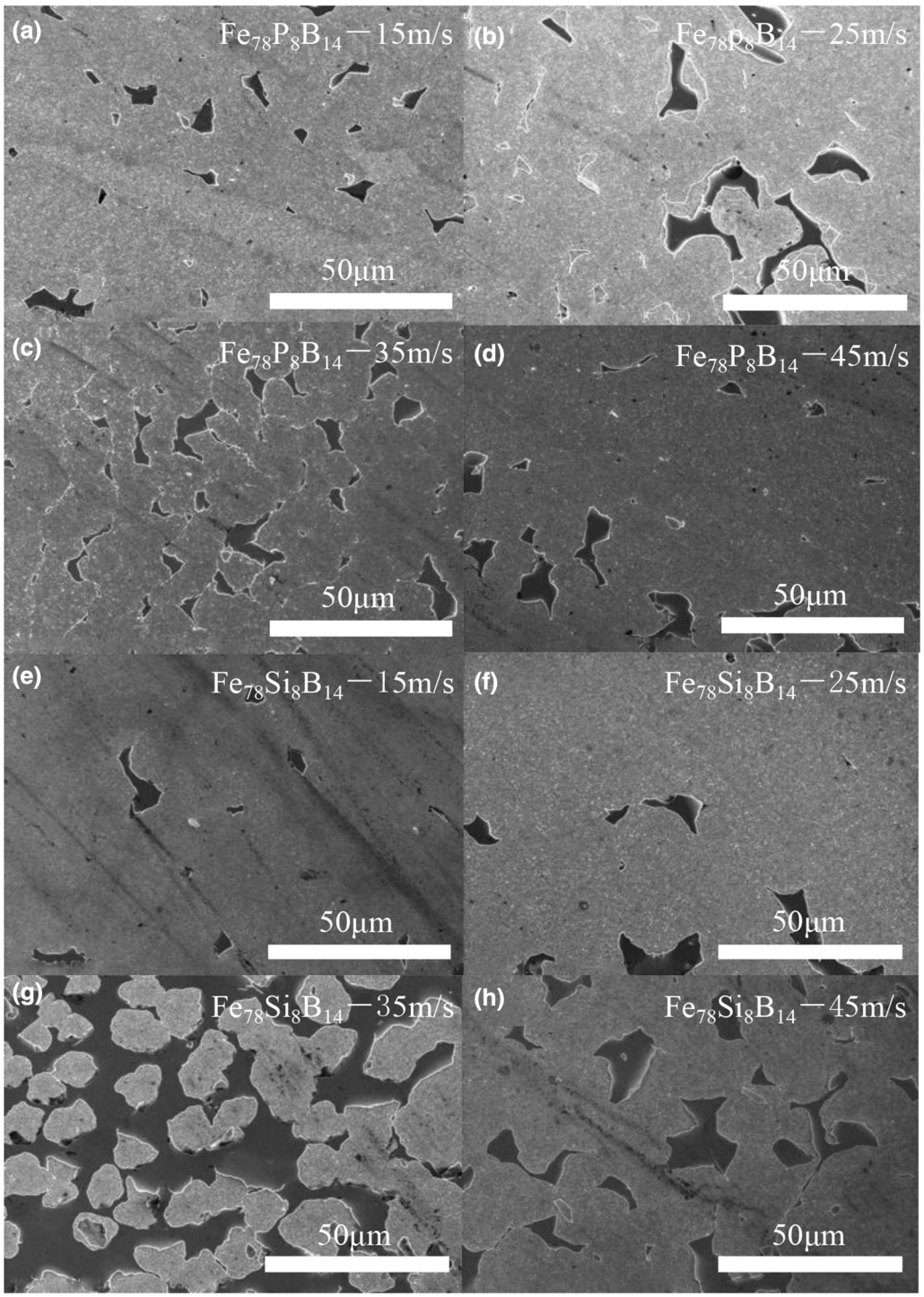


**Fig. 5** SEM images for irradiated $Fe_{78}P_8B_{14}$ (**a–d**) and $Fe_{78}Si_8B_{14}$ (**e–h**) melt-spun ribbons at fluence of $5 \times 10^{17}$ ions/cm$^2$

Previous study indicated that the surface of $Fe_{80}Si_{7.43}B_{12.57}$ amorphous ribbons remains smooth at the fluence of $5 \times 10^{17}$ ions/cm$^2$ when irradiated by 500 keV helium ions [21]. However, significant irradiation-induced damages occur on the surface of $Fe_{78}Si_8B_{14}$ ribbons at the same fluence in present study. It should be emphasized that the composite of current $Fe_{78}Si_8B_{14}$ ribbons is nearly close. However, the incident energy (100 keV) in present experiment is much smaller than that (500 keV) in the literature [21]. Displacements per atom (DPA) is introduced to measure the level of irradiation damage in ribbons [22], which is calculated by TRIM2008. As shown in Fig. 7, the

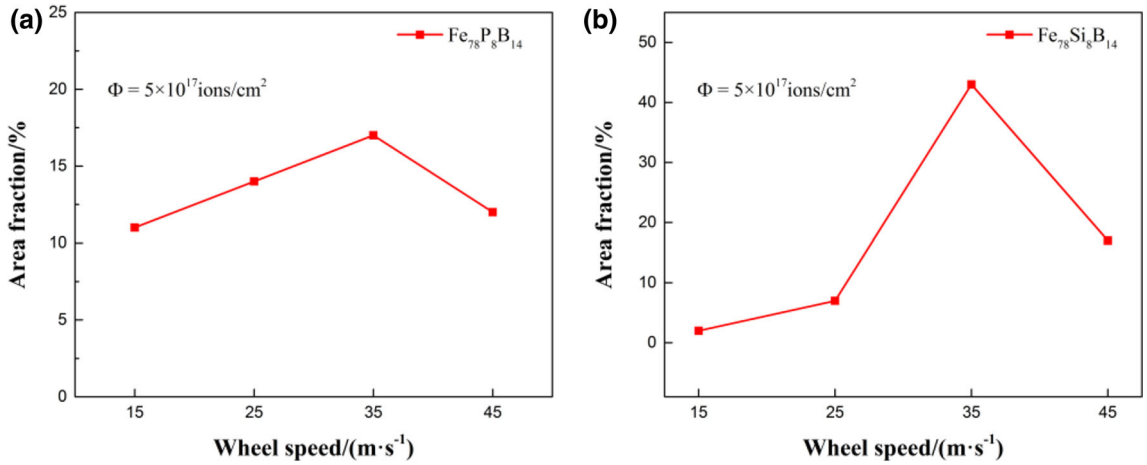


**Fig. 6** Ratio of un-exfoliated area to total irradiated area of $Fe_{78}P_8B_{14}$ (**a**) and $Fe_{78}Si_8B_{14}$ (**b**) melt-spun ribbons

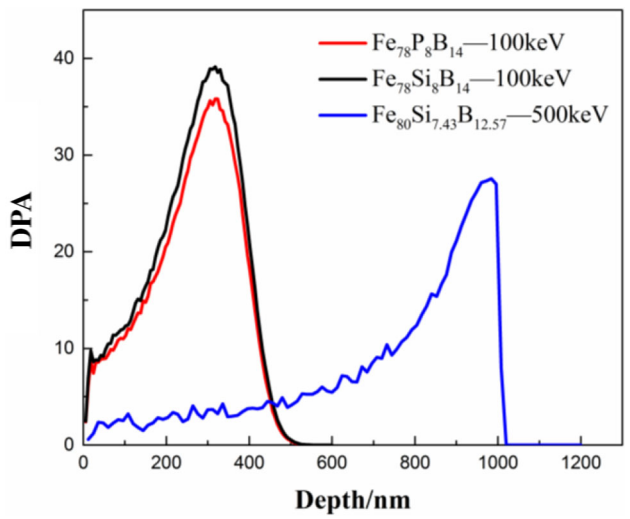


**Fig. 7** SRIM simulation of calculating DPA caused by $He^+$ ion beam irradiation: $Fe_{78}P_8B_{14}$, $Fe_{78}Si_8B_{14}$ and $Fe_{80}Si_{7.43}B_{12.57}$ ($Fe_{80}Si_{7.43}B_{12.57}$ is cited to comparison analysis)

largest DPA value at the lower incident energy is larger than that in higher incident energy. The depth of the largest DPA in lower incident energy is closer to the surface. That means the low-energy ion irradiation is more prone to induce the surface damage.

## 4 Conclusion

The $Fe_{78}Si_8B_{14}$ and $Fe_{78}P_8B_{14}$ ribbons with different wheel speeds were prepared by melt-spinning, and their responses to $He^+$ ion irradiation were investigated. No significant changes on the surface are observed when irradiated at the fluence of $2 \times 10^{17}$ ions/cm$^2$. While at the fluence of $5 \times 10^{17}$ ions/cm$^2$, all ribbons behave the similar irradiation responses in which peeling, flaking and multi-layer damages occur. By calculating the damage area, the melt-spun ribbons at a wheel speed of 35 m/s show the best anti-irradiation performance. The results show the size and a fraction of precipitate phases in amorphous matrix may play a dominated role in resisting the $He^+$ ion irradiation.

**Acknowledgements** The authors would like to acknowledge the support by the National Natural Science Foundation of China (Grant Nos. 51401028, 51271193, 11402277) and the Strategic Priority Research Program of the Chinese Academy of Sciences (Grant No. XDB22 040303). The authors also thank to the support of Opening Fund of State Key Lab of Nuclear Physics and Technology at Peking University.

## References

[1] A.L. Greer, E. Ma, MRS Bull. 32 (2011) 611–619.
[2] M.D. Demetriou, W.L. Johnson, K. Samwer, J. Alloy. Compd. 483 (2009) 644–650.
[3] W.H. Wang, R.J. Wang, F.Y. Li, D.Q. Zhao, M.X. Pan, Appl. Phys. Lett. 74 (1999) 1803–1805.
[4] S.V. Ketov, Y.H. Sun, S. Nachum, Z. Lu, A. Checchi, A.R. Beraldin, H.Y. Bai, W.H. Wang, D.V. Louzguine-Luzgin, M.A. Carpenter, A.L. Greer, Nature 524 (2015) 200–203.
[5] J. Schroers, Adv. Mater. 22 (2010) 1566–1597.
[6] K. Zhang, Z. Hu, F. Li, B. Wei, Appl. Surf. Sci. 390 (2016) 941–945.
[7] N. Nita, R. Schaeublin, M. Victoria, J. Nucl. Mater. 329-333 (2004) 953–957.
[8] Y. Chimi, A. Iwase, N. Ishikawa, J. Nucl. Mater. 297 (2001) 355–357.
[9] M. Rose, A.G. Balogh, H. Hahn, Nucl. Instrum. Methods Phys. Res. Section B 127 (1997) 119–122.
[10] X.M. Bai, A.F. Voter, R.G. Hoagland, Science 327 (2010) 1631–1634.
[11] G. Ackland, Science 327 (2010) 1587–1588.
[12] G.A. Kachurin, M.O. Ruault, A.K. Gutakovsky, Nucl. Instrum. Methods Phys. Res. Section B 147 (1998) 356–360.
[13] M.C. Ridgway, G.D.M. Azevedo, R.G. Elliman, C.J. Glover, D.J. Llewellyn, R. Miller, W. Wesch, G.J. Foran, J. Hansen, A. Nylandsted-Larsen, Phys. Rev. B 71 (2004) 094107.
[14] A. Meldrum, L.A. Boatner, R.C. Ewing, Phys. Rev. Lett. 88 (2002) 025503.

[15] Á. Révész, A. Concustell, L.K. Varga, S. Suriñach, M.D. Baró, Mater. Sci. Eng. A 375-377 (2004) 776–780.
[16] L. Yang, X.T. Zu, Z.G. Wang, F. Gao, X.Y. Wang, H.L. Heinisch, R.J. Kurtz, Nucl. Instrum. Methods Phys. Res. Section B 265 (2007) 541–546.
[17] K. Arakawa, R. Imamura, K. Ohota, K. Ono, J. Appl. Phys. 89 (2001) 4752–4757.
[18] K. Morishita, R. Sugano, B.D. Wirth, T. Diaz de la Rubia, Nucl. Instrum. Methods Phys. Res. Section B 202 (2003) 76–81.
[19] K.Y. Yu, Y. Liu, C. Sun, H. Wang, L. Shao, E.G. Fu, X. Zhang, J. Nucl. Mater. 425 (2012) 140–146.
[20] K. Nagashio, K. Kuribayashi, Acta Mater. 54 (2006) 2353–2360.
[21] W. Hou, X. Mei, Z. Wang, Y. Wang, Nucl. Instrum. Methods Phys. Res. Section B 342 (2015) 221–227.
[22] T.H. Woo, H.S. Cho, Nucl. Instrum. Methods Phys. Res. Section A 652 (2011) 69–72.